Low cortical iron and high entorhinal cortex volume promote cognitive functioning in the oldest-old

van Bergen, Jiri M G ; Li, Xu ; Quevenco, Frances C ; Gietl, Anton F ; Treyer, Valerie ; Leh, Sandra E ; Meyer, Rafael ; Buck, Alfred ; Kaufmann, Philipp A ; Nitsch, Roger M ; van Zijl, Peter C M ; Hock, Christoph ; Unschuld, Paul G

Abstract: The aging brain is characterized by an increased presence of neurodegenerative and vascular pathologies. However, there is substantial variation regarding the relationship between an individual's pathological burden and resulting cognitive impairment. To identify correlates of preserved cognitive functioning at highest age, the relationship between -amyloid plaque load, presence of small vessel cerebrovascular disease (SVCD), iron-burden, and brain atrophy was investigated. Eighty cognitively unimpaired participants (44 oldest-old, aged 85-96 years; 36 younger-old, aged 55-80 years) were scanned by integrated positron emission tomography-magnetic resonance imaging for assessing beta regional amyloid plaque load (18F-flutemetamol), white matter hyperintensities as an indicator of SVCD (fluid-attenuated inversion recovery-magnetic resonance imaging), and iron load (quantitative susceptibility mapping). For the oldest-old group, lower cortical volume, increased -amyloid plaque load, prevalence of SVCD, and lower cognitive performance in the normal range were found. However, compared to normal-old, cortical iron burden was lower in the oldest-old. Moreover, only in the oldest-old, entorhinal cortex volume positively correlated with -amyloid plaque load. Our data thus indicate that the co-occurrence of aging-associated neuropathologies with reduced quantitative susceptibility mapping measures of cortical iron load constitutes a lower vulnerability to cognitive loss.

DOI: https://doi.org/10.1016/j.neurobiolaging.2017.12.014

Accepted Manuscript

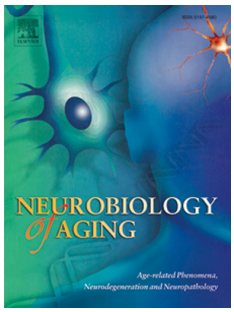

Low cortical iron and high entorhinal cortex volume promote cognitive functioning in the oldest-old

J.M.G. van Bergen, X. Li, F.C. Quevenco, A.F. Gietl, V. Treyer, S.E. Leh, R. Meyer, A. Buck, P.A. Kaufmann, R.M. Nitsch, P.C.M. van Zijl, C. Hock, P.G. Unschuld

PII: S0197-4580(17)30409-8

DOI: 10.1016/j.neurobiolaging.2017.12.014

Reference: NBA 10110

To appear in: *Neurobiology of Aging*

Received Date: 30 March 2017

Revised Date: 9 November 2017

Accepted Date: 13 December 2017

Please cite this article as: van Bergen, J.M.G., Li, X., Quevenco, F.C., Gietl, A.F., Treyer, V., Leh, S.E., Meyer, R., Buck, A., Kaufmann, P.A., Nitsch, R.M., van Zijl, P.C.M., Hock, C., Unschuld, P.G., Low cortical iron and high entorhinal cortex volume promote cognitive functioning in the oldest-old, *Neurobiology of Aging* (2018), doi: 10.1016/j.neurobiolaging.2017.12.014.

Low cortical iron and high entorhinal cortex volume promote cognitive functioning in the oldest-old

J. M. G. van Bergen[1]*, X. Li[2,3], F. C. Quevenco[1], A. F. Gietl[1,4], V. Treyer[1,5], S. E. Leh[4], R. Meyer[1,4], A. Buck[5], P. A. Kaufmann[5], R. M. Nitsch[1,4], P. C. M. van Zijl[2,3], C. Hock[1,4], P. G. Unschuld[1,4]

[1] Institute for Regenerative Medicine, University of Zürich, Switzerland

[2] The Russell H. Morgan Department of Radiology and Radiological Science, Division of MR Research, The Johns Hopkins University School of Medicine, Baltimore, Maryland, USA

[3] F.M. Kirby Research Center for Functional Brain Imaging, Kennedy Krieger Institute, Baltimore, Maryland, USA

[4] Hospital for Psychogeriatric Medicine, University of Zürich, Switzerland

[5] Department of Nuclear Medicine, University Hospital Zürich and University of Zürich, Zürich, Switzerland

*corresponding author:
Jiri van Bergen
Institute for Regenerative Medicine (IREM)
University of Zurich
Minervastrasse 145
CH-8032 Zürich, Switzerland
Switzerland +41-44-3891-453
jiri.vanbergen@uzh.ch

Key words: PET, MRI, beta-Amyloid, iron, QSM, oldest-old, cognitive reserve, maintenance, APOE

Abbreviations

FLAIR = Fluid-attenuated inversion recovery;

QSM = Quantitative susceptibility mapping;

SVCD = small-vessel cerebrovascular disease;

WMH = White matter hyperintensities.

Abstract

The aging brain is characterized by an increased presence of neurodegenerative and vascular pathology. However, there is substantial variation regarding the relationship between an individual's pathological burden and resulting cognitive impairment. To identify correlates of preserved cognitive functioning at highest age, the relationship between β-amyloid plaque-load, presence of small vessel cerebrovascular disease (SVCD), iron-burden and brain atrophy was investigated. 80 cognitively unimpaired participants (44 oldest-old, aged 85-96; 36 younger-old, aged 55-80) were scanned by integrated PET-MRI for assessing β-regional amyloid plaque-load (18F-Flutemetamol), white matter hyperintensities as an indicator of SVCD (FLAIR-MRI) and iron-load (Quantitative Susceptibility Mapping). For the oldest-old group, lower cortical volume, increased β-amyloid plaque-load, prevalence of SVCD and lower cognitive-performance in the normal range was found. However, compared to normal-old, cortical iron burden was lower in the oldest old. Moreover, only in the oldest-old, entorhinal cortex volume positively correlated with β-amyloid plaque-load. Our data thus indicate that the co-occurrence of aging-associated neuropathologies with reduced QSM-measures of cortical iron-load constitutes a lower vulnerability to cognitive loss.

Introduction

While advanced age is associated with substantial brain change and increased risk for cognitive decline, several studies on populations of older adults have revealed high levels of cognitive functioning despite considerable brain pathology. The resilience against such pathologies can be described as the brain's reserve; the cognitive and physiological properties that allow an individual to better tolerate age-related brain alterations and neuropathological burden before cognitive performance is impaired (Barulli and Stern, 2013). Alternatively, maintained cognitive functioning could be attributed not to reserve, but to the presence of neuroprotective factors such as genetic variants, or alterations in clearance mechanisms that prevent the accumulation of neuropathologies at high age (Nyberg et al., 2012). Individuals in the age-group of 85 years and above ("oldest-old") are of particular interest when investigating both the relationship between manifest brain change and risk for Alzheimer's disease (AD) (Kawas et al., 2013), and potential physiological factors that promote resistance against age-related neuropathological burden (Nyberg et al., 2012; Rogalski et al., 2013). While Apolipoprotein E ε4 (APOE4) carrier-status is the strongest known risk factor for sporadic AD in the younger-old (Corder et al., 1993) and has been linked to increased β-amyloid plaque burden in the cognitively normal (Hollands et al., 2017), there also are reports suggesting no association of APOE4 status with incident dementia or compensatory reserve mechanisms in the oldest-old (Corrada et al., 2013; Garibotto et al., 2012).

Several studies have reported substantial discrepancies between measurable neuropathology and expected cognitive performance. This includes increased levels of β-amyloid plaques, which may reflect risk for future cognitive decline due to AD (Kawas et al., 2013; Sperling et al., 2009) and can be measured in cognitively healthy older adults (Mintun et al., 2006). In addition, regional atrophy was linked to AD-associated neurodegenerative brain change, typically affecting hippocampus and entorhinal cortex years before manifestation of cognitive decline (de Leon et al., 1989; Frisoni et al., 2010). The coexistence of β-amyloid plaques with other non-AD specific neurodegenerative alterations could indicate the greatest risk for progression to cognitive decline (Jagust, 2016; Mormino et al., 2014). For example, small-vessel

cerebrovascular disease (SVCD) is a frequent finding in cognitively healthy older adults, and relates to pathogenic markers of AD including β-amyloid plaque burden and regional atrophy, thus increasing risk for cognitive dysfunction (Guzman et al., 2013). Cerebral accumulation of iron is another neuropathological finding associated with aging, but also with neurodegenerative disorders including AD (Ayton et al., 2015; Ayton et al., 2017). Local iron accumulations in the vicinity of β-amyloid plaques may reflect both oxidative stress (Andersen et al., 2014; Meadowcroft et al., 2009; Rottkamp et al., 2001) and presence of activated microglia (Zeineh et al., 2015). Additionally, activated proinflammatory microglia have been correlated to β-amyloid associated neurodegeneration and cognitive impairment (Fan et al., 2017; Serrano-Pozo et al., 2016), suggesting that in vivo measures of iron could indicate both oxidative stress and β-amyloid associated neurodegeneration (Ayton et al., 2017; Derry and Kent, 2017; van Bergen et al., 2016b).

State-of the art neuroimaging using multiple imaging modalities can provide in vivo information on various neuropathological burdens. Radioactive tracers may be used for measuring cerebral β-amyloid plaque burden by Positron-Emission-Tomography (PET) (Klunk et al., 2004; Vandenberghe et al., 2010). T1 weighted MRI is an established measure for regional atrophy in AD (Frisoni et al., 2010) and SVCD severity can be inferred from white matter hyperintensities (WMH), as measured by Fluid-Attenuated Inversion Recovery (FLAIR) MRI (Guzman et al., 2013). Recent developments on quantitative susceptibility mapping (QSM) techniques (Deistung et al., 2013; Li et al., 2011; Lim et al., 2013; Schweser et al., 2012) allow for in vivo measures of cerebral iron-load.

While research on oldest-old populations may significantly advance knowledge on both protective and risk factors in AD and other age-related cognitive disorders (Kawas et al., 2013), not much is known on mechanisms that determine the relationship between presence of major neuropathologies and preserved cognitive functioning in the oldest-old. Aims of the current study therefore were 1.) to assess prevalence of aging-related brain change in a population of cognitively healthy older adults by assessing cerebral β-amyloid burden, differences in structural volume as an indicator of present neurodegenerative change,

cerebral iron-load and the regional distribution of WMH as a proxy of SVCD; 2.) to characterize brain-physiology and neural mechanisms associated with preserved cognitive function, by assessing interactive relationships of pathological alterations and differences between cognitively healthy oldest-old and younger-old.

Methods

Participants

For the current study, two cohorts at the Hospital for Psychogeriatric Medicine and Institute for Regenerative Medicine (IREM), University of Zurich (UZH), Switzerland were combined resulting in a total sample of 80 healthy and cognitively unimpaired older adults. Within the recruited sample, two groups were compared: 36 "younger-old" (ages 55-80 years) and 44 "oldest-old" (ages 85-96 years) participants. Study procedures were in concordance with Human Research Act of Switzerland as well as with the declaration of Helsinki. Written informed consent was obtained from all participants before inclusion in the study.

Inclusion criteria were: preserved everyday functioning and no significant cognitive impairment, as assessed by the CERAD neuropsychological battery (Sotaniemi et al., 2012) and additional tests used in earlier studies of ours (van Bergen et al., 2016b), including Mini Mental State Examination (MMSE), Verbal Learning and Memory Test (VLMT), Boston Naming Test (BNT), Trail Making Test B/A, and Stroop inference test. Exclusion criteria included: significant medication or drug abuse with possible effects on cognition, inability to partake MRI, MRI scans with the evidence of infection or infarction, clinically relevant changes in red blood cell count, serious medical or neuropsychiatric illness and significant exposure to radiation.

MRI data acquisition

All participants were scanned using a 3T GE SIGNA PET-MR whole-body scanner (GE Medical Systems, Milwaukee, WI, USA) equipped with an 8-channel head coil. T1-weighted BRAVO images (TI=450ms, voxel size=1x1x1mm3, flip-angle=12°, ASSET factor=2, scan time=6:00min) were acquired for anatomical referencing and automated image segmentation. MR phase measurements used for QSM calculation were acquired using a multi-echo 3D gradient recalled echo (GRE) sequence with 6 echoes (TR/TE1/ΔTE=40/6/4ms, voxel size=1x1x1mm3, flip angle=15°, bandwidth=±62.5 kHz, flow

compensated, ASSET factor=2, scan time=7:53min). Phase data acquired with an echo time in the range of 18-26ms was used for QSM reconstruction. Images used to determine WMH were acquired using a CUBE FLAIR sequence (TR=6500ms, TE=134, ARC factor=2, voxel size=1x1x1.2mm^3, bandwidth=±31.25 kHz, scan time=6:07min).

Assessment of structure volumes

To assess regional differences, the T1-weighted image was segmented using a multi-atlas matching approach consisting of 143 bilateral Regions of Interest (ROIs) developed as part of the Johns Hopkins University brain atlas. The atlas system is optimized for the parcellation of potential non-healthy brains by applying a Multiple-Atlas Likelihood Fusion algorithm and Ontology Level Control technology on the JHU multi-atlas sets (Djamanakova et al., 2014; Mori et al., 2016; Tang et al., 2013). Specifically, the atlas set of 26 participants aged between 50 and 90 years was used.

To normalize different brain sizes across participants, individual structural volume was corrected with the following approach: *Corrected structure volume = Original structure volume × (whole sample mean intracranial volume / participant intracranial volume)* (van Bergen et al., 2016b). Twelve gray-matter ROIs were selected based on earlier reports on distribution of brain pathology at early stages of AD (Frisoni et al., 2010; Serrano-Pozo et al., 2011).

ROI-masks were eroded with two pixels to account for partial volume effects before being used as a mask to analyze average iron-load (QSM), β-amyloid burden and WMH detection. These imaging volumes were first re-sliced to the individual's T1 space, in which the atlas was defined, before further analysis.

Quantitative susceptibility mapping (QSM) for measuring brain iron-load

Multiple processing steps were performed to calculate from the acquired MR phase images the quantitative susceptibility maps of which local cerebral iron-load was assessed. First, phase unwrapping was performed using Laplacian based phase unwrapping (Li et al., 2011). A brain mask was then obtained by skull-stripping the GRE magnitude image acquired at TE of 14ms using FSL's brain extraction tool

(BET, FMRIB Oxford, UK). The unwrapped phase images were then divided by 2π*TE to obtain an image of the frequency shift in Hz for each echo. Subsequently, background fields were eliminated with the sophisticated harmonic artifact reduction for phase data (SHARP) (Schweser et al., 2011) approach using a variable spherical kernel size with a maximum radius of 4mm and a regularization parameter of 0.05 (Schweser et al., 2011; Wu et al., 2012b). After removal of background fields, the resulting images of the three echoes were averaged to obtain a higher SNR as compared to single echo reconstruction (Wu et al., 2012a). Inverse dipole calculations to obtain the susceptibility maps were performed using an iLSQR based minimization (Li et al., 2015). The means of the standard deviations of susceptibility in commonly accepted QSM reference regions, such as various white matter bundles and sections of the cerebrospinal fluid, were evaluated to select the region with the lowest mean standard deviations as the reference region (Deistung et al., 2013). For clarity and consistency with earlier studies, changes in susceptibility values will be referred to as changes in iron-load, due to the previously demonstrated correlation of susceptibility values with tissue iron-load in brain gray matter (Deistung et al., 2013; Li et al., 2011; Lim et al., 2013; Schweser et al., 2012).

Flutemetamol-PET for estimation of brain β-amyloid plaque burden

Flutemetamol-PET was used to estimate individual local brain β-amyloid plaque burden (Vandenberghe et al., 2010). Individual dose of 140MBq of Flutemetamol was injected into the cubital vein. Time-of-flight algorithm including necessary corrections were applied to reconstruct the PET-images. Standard MRAC images were used to derive attenuation correction maps according standard implemented algorithms. Late frame (minutes 85-105) values were standardized by the cerebellar gray matter value (Vandenberghe et al., 2010), resulting in 3D-volumes of Flutemetamol retention as an estimate of β-amyloid burden via standard uptake value ratios (SUVR) (matrix=256x256x89, voxel size=1.2x1.2x2.78mm^3).

Single measures of individual cortical β-amyloid burden and iron-load were calculated for each participant based on average gray-matter ROI values of Flutemetamol-SUVR and susceptibility,

respectively, as reported earlier (van Bergen et al., 2016b). To determine "amyloid-positive" status the Flutemetamol-SUVR cutoff value of 1.562 was used (Vandenberghe et al., 2010).

Assessment of SVCD by semi-automated WMH detection

To assess occurrence of WMH, each participant's FLAIR images were segmented into gray matter and white matter regions using the previously generated atlas. Parameters necessary for labeling atlas regions with WMH were determined by repeatedly manually optimizing the automated process. In a subset of 10 randomly selected participants all white matter regions exhibiting WMH were manually labeled to create a training dataset. Of the 110 white matter regions defined by the atlas, regions smaller than 1 ml were excluded as they were found to not be validly labeled by the automated process when optimizing the algorithm by comparison to manual assessment. This resulted in a total of 42 white matter regions where automated labeling was consistent with manual labeling in the training dataset (average corrected structure volume and standard deviation 5.17 ± 1.70 ml). All gray matter regions were grouped together to extract the average gray matter intensity per participant. As demonstrated earlier (Iorio et al., 2013), presence of WMH in each white matter region was automatically identified by counting voxels with intensities 1.5 standard deviation above the average gray matter intensity of each participant. Finally, regions including more than 0.25 ml of voxels identified as representing WMH, were labeled as exhibiting WMH. The threshold of 0.25 ml was determined by comparing manual with automated labeling for maximizing specificity in the training dataset. Automated WMH assessment was finalized by manual validation of identified regions. This included adjustment of WMH counts when a region solely contained the edge of a single WMH while the core of that WMH was in another region. By summing the number of regions labeled as exhibiting WMH, a value indicating SVCD-burden was calculated for each participant.

Local correlation analysis

For each of the selected ROIs, WMH score and regional volume were used as outcome variables with local β-amyloid burden and local iron-load as predictors, while controlling for age and gender. All correlation analyses were performed using Spearman's rank correlation coefficient. To investigate differences in the correlation effects between oldest-old and younger-old, Fisher's r-to-z transformation was applied on the correlation coefficients within each region for each group (Fisher, 1921). False Discovery Rate (FDR) correction for multiple testing (Benjamini and Hochberg, 1995) was applied to the p-values of all regions for each predictor-outcome pair and results were found significant when p-FDR-corrected < 0.05. Two-sided t-tests were used for group comparisons. In case of non-normal distributed data, statistical tests for differences between groups were performed on log-transformed data. All statistical tests were performed in MATLAB R2016b (Mathworks, Natick, MA).

Results

Characteristics of the studied populations and neuropsychological performance.

Demographic information for the investigated study populations and neuropsychological test performance at time of inclusion are summarized in **table 1**. The average education level, as measured by years of formal education, was significantly lower in oldest-old compared to younger-old (oldest-old: 14.2 (2.8) years; younger-old: 15.9 (2.6), p=0.010). Clinical examination revealed self-reliance and absence of cognitive impairment in the oldest-old group. However, they performed significantly lower than the younger-old group in all administered neuropsychological tests except CERAD word list recognition (**table 1B**). Eleven out of 36 younger-old (31%) and six out of 44 oldest-old (14%) were APOE4 carriers. Fisher test on the odds ratio of an APOE4 carrier having oldest-old status resulted in a non-significant trend (p=0.071, CI=0.11-1.09).

Prevalence of neuropathological burden in oldest- versus younger-old.

While corrected structure volume in cortical gray matter regions and the hippocampus was significantly lower in oldest-old compared to younger-old, no significant difference could be observed for the entorhinal cortex (**figure 1A**, **supplementary table 1A**). The cutoff for Flutemetamol SUVR (Vandenberghe et al., 2010) identified eight oldest-old and five younger-old participants as "amyloid-positive". Consistently, quantitative assessment of Flutemetamol SUVR indicated significantly higher regional β-amyloid plaque burden in the oldest-old than younger-old for all twelve investigated brain structures (**figure 1B**, **supplementary table 1B**). Deep frontal white matter was found to have the lowest average susceptibility standard deviations and was selected as a reference region to assess relative iron-load for each participant. Interestingly, iron-load in the oldest-old was significantly lower in neocortical regions, insula and posterior cingulate. Only in the putamen was iron-load higher in oldest-old than the younger-old (**figure 2, supplementary table 1C**). As SVCD-burden was non-normally distributed, group comparisons were performed on log-transformed scores. Almost all oldest-old exhibited substantial

SVCD upon visual inspection, which is reflected by significantly higher (p=0.004) SVCD in oldest-old (6.59 ± 0.62) compared to younger-old (2.36 ± 0.29, **supplementary table 1D)**. For assessment of effects accountable to age, a 1-way MANCOVA with age as covariate was used to compare neuropsychological test scores, volume, cortical β-amyloid burden, cortical iron and log-transformed SVCD-burden between oldest-old and younger-old. Here, no significant difference could be observed, when correcting for age.

Relationship between β-amyloid burden, iron-load, structure volume and prevalence of SVCD.

Significant correlations (p-FDR-corrected<0.05) in the whole sample were found between β-amyloid burden and structure volume in the amygdala; and between iron-load and structure volume in insula, entorhinal cortex and parietal cortex (**table 2A**). Prevalence of SVCD correlated with β-amyloid burden in the entorhinal cortex and frontal cortex. Moreover, SVCD correlated negatively with iron-load in the amygdala, entorhinal cortex, parietal cortex and the neocortex as a whole (**table 2B**). When testing APOE4 carriers separately, significant correlations between β-amyloid burden and SVCD (p=0.01 r=0.80) and iron-load and volume (p=0.02 r=-0.60) could be observed in the entorhinal cortex.

Group-specific correlations of structure volume with β-amyloid burden.

Secondary, group specific regression-analysis indicated a significant correlation of high local β-amyloid burden with high structure volume in the entorhinal cortex of the oldest-old, which was not present in the younger-old (**figure 3**, oldest-old p=0.01 r=0.39, younger-old p=0.59 r=-0.09) and insula (oldest-old p=0.04 r=0.31, younger-old p=0.31 r=-0.18), significant difference of correlations was confirmed by Fisher's r-to-z transformation (entorhinal cortex p=0.031, insula p=0.032).

To identify potential effects of education level, correlation analysis was performed with local structure volume and local β-amyloid burden as outcome variables and years of education as predictor, while controlling for age and gender. No significant correlation with years of education was found in any of the structures (**supplementary table 2**).

Discussion

By investigating a study population of cognitively unimpaired younger- and oldest-old by combined PET-MRI, we found significantly higher prevalence of neuropathological burden in the oldest-old, as reflected by cerebral β-amyloid burden, reduced volume of structures and higher prevalence of SVCD. While neuropsychological testing indicated generally lower performance levels in the oldest-old, they did not show significant cognitive impairment. Differences in the oldest-old furthermore included lower iron-load in cortical regions and an association of high entorhinal volume with entorhinal β-amyloid burden. Our findings support earlier considerations that distinct physiological brain properties may allow for maintained high cognitive functioning in the oldest-old, despite present brain pathology (Barulli and Stern, 2013; Nyberg et al., 2012). To our knowledge, this is the first report indicating that reduced QSM measures of cortical iron-load constitute a lower vulnerability to loss of cognitive function at highest age.

Amyloid-PET tracers, such as 18F-Flutemetamol (Vandenberghe et al., 2010), have become an established approach to estimate regional β-amyloid burden in AD-risk populations. Differences in brain structure volumes were investigated by applying a multi-atlas matching approach to T1-MRI data, using Likelihood Fusion and Ontology Level Control algorithms, as validated for both healthy and diseased study populations (Djamanakova et al., 2014; Tang et al., 2013). Recent efforts in validation of the QSM technology made it possible to quantitatively assess regional iron-load in vivo (Deistung et al., 2013; Langkammer et al., 2012) and assess iron in a context of neurodegenerative disease (Acosta-Cabronero et al., 2013; Ayton et al., 2017; van Bergen et al., 2016a; van Bergen et al., 2016b). When interpreting the susceptibility data, it needs to be considered that the iron-load could vary on an inter-voxel basis and that QSM is biased by decreased myelin density (Langkammer et al., 2012; Liu et al., 2011). However, the cortical and deep gray matter regions investigated in this study are low in myelin content and thus the myelin contribution was considered minimal. Distortion by processes of co-registration of PET with MR-indicators of neuropathological burden or bias due to changes occurring in the time between PET and MR

acquisition could be avoided as the respective measures were acquired using an integrated PET-MR instrument.

When investigating the entire study sample, a significant relationship between β-amyloid burden and reduced volume resulted, which appears consistent with earlier reports on biomarker-associations in populations of older adults at risk for AD (Frisoni et al., 2010; Mormino et al., 2014). Our observation of SVCD correlating with β-amyloid burden concurs with earlier ADNI-findings (Guzman et al., 2013). Interestingly, we find negative correlations between iron and SVCD throughout the brain - which surprised us, as we expected SVCD to be associated with paramagnetic properties due to extravasated hemoglobin and vascular pathology. Our SVCD measure did not include the size but only the occurrence of WMH as a reflection of incidence of vascular breakdown. As we cannot exclude that an analysis focused on WMH-size may provide different results, at this point our findings on SVCD in a context of iron need to be interpreted with caution. Additional studies are needed to validate the use of the here-applied WMH score for assessing SVCD, and also should allow for potential roles of activated microglia and iron clearing mechanisms. Our finding of substantial neuropathological burden in the oldest-old is consistent with earlier studies on high aged populations (Kawas et al., 2013). In general, reduced structural volume and increased β-amyloid burden were more pronounced in the oldest-old than in the younger-old, in line with earlier findings of reduced volume as an indicator of incipient neurodegeneration and cognitive decline (Dekhtyar et al., 2017; Frisoni et al., 2010; Mormino et al., 2014). The oldest-old population in our study showed a generally lower cognitive performance than the younger-old, which appears consistent with earlier reports on non-pathological cognitive change during aging. Oldest-old status in our sample was associated with fewer years of formal education, which reflects the lower availability of higher-education in Switzerland during adolescence of the very old participants. It is not expected that formal education influence results at this stage of their life, this is supported by the lack of correlation between years of education and β-amyloid burden or structure volume. Additionally, we only found a non-significant trend regarding the effect of APOE4 status for the odds of being oldest-

old versus younger-old. This finding could be due to insufficient power in our sample. Alternatively, it might be consistent with earlier reports that suggest other factors of brain physiology beyond APOE4 determine cognitive functioning at a very high age (Corrada et al., 2013; Garibotto et al., 2012). The fact that our oldest-old population exhibited a high degree of cognitive functionality despite present neuropathology concurs with earlier observations of preserved cognition at highest age (Nyberg et al., 2012; Rogalski et al., 2013). Considering the well-established relationship between high β-amyloid burden and risk for cognitive decline during aging (Jansen et al., 2015), our finding of significantly higher β-amyloid burden in cognitively unimpaired oldest-old participants suggests particular resilience against neuropathology. Here, our findings of lower iron-load in brain regions implicated in cognitive processes, such as the neocortex, posterior cingulate and insula, potentially reflect less neuronal damage. Pathological processes that are considered to be reflected by increased local iron-load include oxidative stress and presence of activated microglia (Meadowcroft et al., 2009; Nunez et al., 2012; Rottkamp et al., 2001; Serrano-Pozo et al., 2016; Zeineh et al., 2015). Moreover, increased iron-load is a frequent finding in neurodegenerative disease (Andersen et al., 2014; Kruer, 2013). Increased iron-load in basal ganglia structures, particularly the putamen, are a known effect of aging (Bartzokis et al., 1997; Hallgren and Sourander, 1958) and are consistent with the spatial distribution of our QSM measures of local iron-load. Our observation of low cortical iron-load in the cognitively unimpaired oldest-old might thus reflect lower vulnerability to age-related neuropathology, and may be consistent with reports of elevated brain iron being associated with mild cognitive impairment and liability for AD (Ayton et al., 2015; Ayton et al., 2017; Derry and Kent, 2017; van Bergen et al., 2016b). Furthermore, our findings are consistent with recently published data on a relationship between increased QSM measures of cerebral iron and β-amyloid associated cognitive decline (Ayton et al., 2017).

Several studies have investigated changes to the entorhinal cortex associated with aging and incipient AD, as indicated by reduced structural volume (de Leon et al., 1989; Frisoni et al., 2010), and found that increased structural volume of memory regions promotes maintained cognitive performance (Dekhtyar et

al., 2017; deToledo-Morrell et al., 2004). Thus, while the current clinical study does not provide information on neurobiological mechanisms, the here reported positive relationship between entorhinal structural volume and β-amyloid plaque-density, which was only observable in the oldest-old, might indicate lower vulnerability. However, as entorhinal cortex volumes in the oldest-old did not differ from the younger-old, this finding needs to be interpreted with caution.

Taken together, by investigating a cross-sectional sample of younger- and oldest-old, we provide neuroimaging-evidence that low cortical iron-load and high entorhinal volume despite high β-amyloid burden might characterize individuals less affected by aging-associated neuropathologies. Additional translational studies are needed to characterize the interplay between molecular mechanisms and genetic disposition that allows for maintained cognitive function at highest age. While our findings are consistent with recent reports on low iron burden as a predictor of preserved cognitive functioning in older adults (Ayton et al., 2017), therapeutic trials are needed to investigate whether these correlates of individual resilience may be exploited for specific disease modifying intervention.

Figure captions

Figure 1) Mean regional average values (SEM) per group for **A)** volume (ml), **B)** β-amyloid plaque burden (18F-Flutemetamol SUVR). Significant differences after FDR-multiple-testing-correction are indicated by * = $p < 0.05$, ** = $p < 0.01$ and *** = $p < 0.001$.

Figure 2) Mean regional average values (SEM) per group for iron (susceptibility, ppm). Significant differences after FDR multiple testing correction are indicated by * = $p < 0.05$, ** = $p < 0.01$ and *** = $p < 0.001$.

Figure 3) Scatterplot for correlations between entorhinal volume (ml) and entorhinal β-amyloid plaque burden for oldest-old ($r=0.39$, $p=0.01$), younger-old $r=-0.09$, $p=0.59$.

Acknowledgments

We thank all participants for their study participation and Esmeralda Gruber for help with patient recruitment and study administration. This work was funded by the Swiss National Science Foundation (Schweizerischer Nationalfonds, SNF), the Mäxi foundation, the Clinical Research Priority Program (CRPP) of the University of Zürich on Molecular Imaging (MINZ), a grant from the National Institutes of Health (NIBIB) P41 EB015909, investigator initiated research support by GE-healthcare (114-2014-IIR-0075 and 114-2014-IIR-0076), and institutional support from the Institute for Regenerative Medicine (IREM), University of Zürich, Switzerland. This work was supported by the Zürich Impulse Program for the Sustainable Development of Mental Health Services.

Competing Financial Interests statement

Dr. Peter van Zijl is a paid lecturer for Philips Healthcare and is the inventor of technology that is licensed to Philips. This arrangement has been approved by The Johns Hopkins University in accordance with its Conflict of Interest policies. Dr. Paul G. Unschuld is supported by a GE-healthcare grant for investigator initiated research. This funding is in accordance with guidelines issued by the University of Zürich.

References

Acosta-Cabronero, J., Williams, G.B., Cardenas-Blanco, A., Arnold, R.J., Lupson, V., Nestor, P.J., 2013. In vivo quantitative susceptibility mapping (QSM) in Alzheimer's disease. PLoS ONE 8(11), e81093-e81093.

Andersen, H.H., Johnsen, K.B., Moos, T., 2014. Iron deposits in the chronically inflamed central nervous system and contributes to neurodegeneration. Cell Mol Life Sci 71(9), 1607-1622.

Ayton, S., Faux, N.G., Bush, A.I., Alzheimer's Disease Neuroimaging, I., 2015. Ferritin levels in the cerebrospinal fluid predict Alzheimer's disease outcomes and are regulated by APOE. Nat Commun 6, 6760.

Ayton, S., Fazlollahi, A., Bourgeat, P., Raniga, P., Ng, A., Lim, Y.Y., Diouf, I., Farquharson, S., Fripp, J., Ames, D., Doecke, J., Desmond, P., Ordidge, R., Masters, C.L., Rowe, C.C., Maruff, P., Villemagne, V.L., Salvado, O., Bush, A.I., Life, A.I.B., 2017. Cerebral quantitative susceptibility mapping predicts amyloid-beta-related cognitive decline. Brain 140, 2112-2119.

Bartzokis, G., Beckson, M., Hance, D.B., Marx, P., Foster, J.A., Marder, S.R., 1997. MR evaluation of age-related increase of brain iron in young adult and older normal males. Magn Reson Imaging 15(1), 29-35.

Barulli, D., Stern, Y., 2013. Efficiency, capacity, compensation, maintenance, plasticity: emerging concepts in cognitive reserve. Trends Cogn Sci 17(10), 502-509.

Benjamini, Y., Hochberg, Y., 1995. Controlling the False Discovery Rate: A Practical and Powerful Approach to Multiple Testing. pp. 289-300.

Corder, E.H., Saunders, a.M., Strittmatter, W.J., Schmechel, D.E., Gaskell, P.C., Small, G.W., Roses, a.D., Haines, J.L., Pericak-Vance, M.a., 1993. Gene dose of apolipoprotein E type 4 allele and the risk of Alzheimer's disease in late onset families. Science (New York, N.Y.) 261(5123), 921-923.

Corrada, M.M., Paganini-Hill, A., Berlau, D.J., Kawas, C.H., 2013. Apolipoprotein E genotype, dementia, and mortality in the oldest old: the 90+ Study. Alzheimers Dement 9(1), 12-18.

de Leon, M.J., George, A.E., Stylopoulos, L.A., Smith, G., Miller, D.C., 1989. Early marker for Alzheimer's disease: the atrophic hippocampus. Lancet 2(8664), 672-673.

Deistung, A., Schafer, A., Schweser, F., Biedermann, U., Turner, R., Reichenbach, J.R., 2013. Toward in vivo histology: a comparison of quantitative susceptibility mapping (QSM) with magnitude-, phase-, and R2*-imaging at ultra-high magnetic field strength. Neuroimage 65, 299-314.

Dekhtyar, M., Papp, K.V., Buckley, R., Jacobs, H.I.L., Schultz, A.P., Johnson, K.A., Sperling, R.A., Rentz, D.M., 2017. Neuroimaging markers associated with maintenance of optimal memory performance in late-life. Neuropsychologia 100, 164-170.

Derry, P.J., Kent, T.A., 2017. Correlating quantitative susceptibility mapping with cognitive decline in Alzheimer's disease. Brain 140(8), 2069-2072.

deToledo-Morrell, L., Stoub, T.R., Bulgakova, M., Wilson, R.S., Bennett, D.A., Leurgans, S., Wuu, J., Turner, D.A., 2004. MRI-derived entorhinal volume is a good predictor of conversion from MCI to AD. Neurobiol Aging 25(9), 1197-1203.

Djamanakova, A., Tang, X., Li, X., Faria, A.V., Ceritoglu, C., Oishi, K., Hillis, A.E., Albert, M., Lyketsos, C., Miller, M.I., Mori, S., 2014. Tools for multiple granularity analysis of brain MRI data for individualized image analysis. Neuroimage 101, 168-176.

Fan, Z., Brooks, D.J., Okello, A., Edison, P., 2017. An early and late peak in microglial activation in Alzheimer's disease trajectory. Brain 140(3), 792-803.

Fazekas, F., Chawluk, J.B., Alavi, A., Hurtig, H.I., Zimmerman, R.A., 1987. Mr Signal Abnormalities at 1.5-T in Alzheimers Dementia and Normal Aging. American Journal of Neuroradiology 8(3), 421-426.

Fisher, R.a., 1921. On the 'probable error' of coefficient of correlations deduced from a small sample. Metron 1, 1-32.

Frisoni, G.B., Fox, N.C., Jack, C.R., Jr., Scheltens, P., Thompson, P.M., 2010. The clinical use of structural MRI in Alzheimer disease. Nat Rev Neurol 6(2), 67-77.

Garibotto, V., Borroni, B., Sorbi, S., Cappa, S.F., Padovani, A., Perani, D., 2012. Education and occupation provide reserve in both ApoE epsilon4 carrier and noncarrier patients with probable Alzheimer's disease. Neurol Sci 33(5), 1037-1042.

Guzman, V.A., Carmichael, O.T., Schwarz, C., Tosto, G., Zimmerman, M.E., Brickman, A.M., Alzheimer's Disease Neuroimaging, I., 2013. White matter hyperintensities and amyloid are independently associated with entorhinal cortex volume among individuals with mild cognitive impairment. Alzheimers Dement 9(5 Suppl), S124-131.

Hallgren, B., Sourander, P., 1958. The effect of age on the non-haemin iron in the human brain. Journal of neurochemistry 3(1), 41-51.

Hollands, S., Lim, Y.Y., Laws, S.M., Villemagne, V.L., Pietrzak, R.H., Harrington, K., Porter, T., Snyder, P., Ames, D., Fowler, C., Rainey-Smith, S.R., Martins, R.N., Salvado, O., Robertson, J., Rowe, C.C., Masters, C.L., Maruff, P., Group, A.R., 2017. APOEvarepsilon4 Genotype, Amyloid, and Clinical Disease Progression in Cognitively Normal Older Adults. J Alzheimers Dis.

Iorio, M., Spalletta, G., Chiapponi, C., Luccichenti, G., Cacciari, C., Orfei, M.D., Caltagirone, C., Piras, F., 2013. White matter hyperintensities segmentation: a new semi-automated method. Front Aging Neurosci 5, 76.

Jagust, W., 2016. Is amyloid-beta harmful to the brain? Insights from human imaging studies. Brain 139(Pt 1), 23-30.

Jansen, W.J., Ossenkoppele, R., Knol, D.L., Tijms, B.M., Scheltens, P., Verhey, F.R., Visser, P.J., Amyloid Biomarker Study, G., Aalten, P., Aarsland, D., Alcolea, D., Alexander, M., Almdahl, I.S., Arnold, S.E., Baldeiras, I., Barthel, H., van Berckel, B.N., Bibeau, K., Blennow, K., Brooks, D.J., van Buchem, M.A., Camus, V., Cavedo, E., Chen, K., Chetelat, G., Cohen, A.D., Drzezga, A., Engelborghs, S., Fagan, A.M., Fladby, T., Fleisher, A.S., van der Flier, W.M., Ford, L., Forster, S., Fortea, J., Foskett, N., Frederiksen, K.S., Freund-Levi, Y., Frisoni, G.B., Froelich, L., Gabryelewicz, T., Gill, K.D., Gkatzima, O., Gomez-Tortosa, E., Gordon, M.F., Grimmer, T., Hampel, H., Hausner, L., Hellwig, S., Herukka, S.K., Hildebrandt, H., Ishihara, L., Ivanoiu, A., Jagust, W.J., Johannsen, P., Kandimalla, R., Kapaki, E., Klimkowicz-Mrowiec, A., Klunk, W.E., Kohler, S., Koglin, N., Kornhuber, J., Kramberger, M.G., Van Laere, K., Landau, S.M., Lee, D.Y., de Leon, M., Lisetti, V., Lleo, A., Madsen, K., Maier, W., Marcusson, J., Mattsson, N., de Mendonca, A., Meulenbroek, O., Meyer, P.T., Mintun, M.A., Mok, V., Molinuevo, J.L., Mollergard, H.M., Morris, J.C., Mroczko, B., Van der Mussele, S., Na, D.L., Newberg, A., Nordberg, A., Nordlund, A., Novak, G.P., Paraskevas, G.P., Parnetti, L., Perera, G., Peters, O., Popp, J., Prabhakar, S., Rabinovici, G.D., Ramakers, I.H., Rami, L., Resende de Oliveira, C., Rinne, J.O., Rodrigue, K.M., Rodriguez-Rodriguez, E., Roe, C.M., Rot, U., Rowe, C.C., Ruther, E., Sabri, O., Sanchez-Juan, P., Santana, I., Sarazin, M., Schroder, J., Schutte, C., Seo, S.W., Soetewey, F., Soininen, H., Spiru, L., Struyfs, H., Teunissen, C.E., Tsolaki, M., Vandenberghe, R., Verbeek, M.M., Villemagne, V.L., Vos, S.J., van Waalwijk van Doorn, L.J., Waldemar, G., Wallin, A., Wallin, A.K., Wiltfang, J., Wolk, D.A., Zboch, M., Zetterberg, H., 2015. Prevalence of cerebral amyloid pathology in persons without dementia: a meta-analysis. JAMA 313(19), 1924-1938.

Kawas, C.H., Greenia, D.E., Bullain, S.S., Clark, C.M., Pontecorvo, M.J., Joshi, A.D., Corrada, M.M., 2013. Amyloid imaging and cognitive decline in nondemented oldest-old: the 90+ Study. Alzheimers Dement 9(2), 199-203.

Klunk, W.E., Engler, H., Nordberg, A., Wang, Y., Blomqvist, G., Holt, D.P., Bergstrom, M., Savitcheva, I., Huang, G.F., Estrada, S., Ausen, B., Debnath, M.L., Barletta, J., Price, J.C., Sandell, J., Lopresti, B.J., Wall, A., Koivisto, P., Antoni, G., Mathis, C.A., Langstrom, B., 2004. Imaging brain amyloid in Alzheimer's disease with Pittsburgh Compound-B. Ann Neurol 55(3), 306-319.

Kruer, M.C., 2013. The neuropathology of neurodegeneration with brain iron accumulation. International review of neurobiology 110, 165-194.

Langkammer, C., Schweser, F., Krebs, N., Deistung, A., Goessler, W., Scheurer, E., Sommer, K., Reishofer, G., Yen, K., Fazekas, F., Ropele, S., Reichenbach, J.R., 2012. Quantitative susceptibility mapping (QSM) as a means to measure brain iron? A post mortem validation study. Neuroimage 62(3), 1593-1599.

Li, W., Wang, N., Yu, F., Han, H., Cao, W., Romero, R., Tantiwongkosi, B., Duong, T.Q., Liu, C., 2015. A method for estimating and removing streaking artifacts in quantitative susceptibility mapping. Neuroimage 108, 111-122.
Li, W., Wu, B., Liu, C., 2011. Quantitative susceptibility mapping of human brain reflects spatial variation in tissue composition. Neuroimage 55(4), 1645-1656.
Lim, I.A., Faria, A.V., Li, X., Hsu, J.T., Airan, R.D., Mori, S., van Zijl, P.C., 2013. Human brain atlas for automated region of interest selection in quantitative susceptibility mapping: application to determine iron content in deep gray matter structures. Neuroimage 82, 449-469.
Liu, C., Li, W., Johnson, G.A., Wu, B., 2011. High-field (9.4T) MRI of brain dysmyelination by quantitative mapping of magnetic susceptibility. NeuroImage 56(3), 930-938.
Meadowcroft, M.D., Connor, J.R., Smith, M.B., Yang, Q.X., 2009. MRI and histological analysis of beta-amyloid plaques in both human Alzheimer's disease and APP/PS1 transgenic mice. J Magn Reson Imaging 29(5), 997-1007.
Mintun, M.A., Larossa, G.N., Sheline, Y.I., Dence, C.S., Lee, S.Y., Mach, R.H., Klunk, W.E., Mathis, C.A., DeKosky, S.T., Morris, J.C., 2006. [11C]PIB in a nondemented population: potential antecedent marker of Alzheimer disease. Neurology 67(3), 446-452.
Mori, S., Wu, D., Ceritoglu, C., Li, Y., Kolasny, A., Vaillant, M.A., Faria, A.V., Oishi, K., Miller, M.I., 2016. MRICloud: Delivering High-Throughput MRI Neuroinformatics as Cloud-Based Software as a Service. Comput Sci Eng 18(5), 21-35.
Mormino, E.C., Betensky, R.A., Hedden, T., Schultz, A.P., Amariglio, R.E., Rentz, D.M., Johnson, K.A., Sperling, R.A., 2014. Synergistic effect of beta-amyloid and neurodegeneration on cognitive decline in clinically normal individuals. JAMA Neurol 71(11), 1379-1385.
Nunez, M.T., Urrutia, P., Mena, N., Aguirre, P., Tapia, V., Salazar, J., 2012. Iron toxicity in neurodegeneration. Biometals 25(4), 761-776.
Nyberg, L., Lovden, M., Riklund, K., Lindenberger, U., Backman, L., 2012. Memory aging and brain maintenance. Trends Cogn Sci 16(5), 292-305.
Rogalski, E.J., Gefen, T., Shi, J., Samimi, M., Bigio, E., Weintraub, S., Geula, C., Mesulam, M.M., 2013. Youthful memory capacity in old brains: anatomic and genetic clues from the Northwestern SuperAging Project. J Cogn Neurosci 25(1), 29-36.
Rottkamp, C.A., Raina, A.K., Zhu, X., Gaier, E., Bush, A.I., Atwood, C.S., Chevion, M., Perry, G., Smith, M.A., 2001. Redox-active iron mediates amyloid-beta toxicity. Free Radic Biol Med 30(4), 447-450.
Schweser, F., Deistung, A., Lehr, B.W., Reichenbach, J.R., 2011. Quantitative imaging of intrinsic magnetic tissue properties using MRI signal phase: an approach to in vivo brain iron metabolism? Neuroimage 54(4), 2789-2807.
Schweser, F., Sommer, K., Deistung, A., Reichenbach, J.R., 2012. Quantitative susceptibility mapping for investigating subtle susceptibility variations in the human brain. Neuroimage 62(3), 2083-2100.
Serrano-Pozo, A., Betensky, R.A., Frosch, M.P., Hyman, B.T., 2016. Plaque-Associated Local Toxicity Increases over the Clinical Course of Alzheimer Disease. Am J Pathol 186(2), 375-384.
Serrano-Pozo, A., Frosch, M.P., Masliah, E., Hyman, B.T., 2011. Neuropathological alterations in Alzheimer disease. Cold Spring Harb Perspect Med 1(1), a006189.
Sotaniemi, M., Pulliainen, V., Hokkanen, L., Pirttila, T., Hallikainen, I., Soininen, H., Hanninen, T., 2012. CERAD-neuropsychological battery in screening mild Alzheimer's disease. Acta Neurol Scand 125(1), 16-23.
Sperling, R.A., Laviolette, P.S., O'Keefe, K., O'Brien, J., Rentz, D.M., Pihlajamaki, M., Marshall, G., Hyman, B.T., Selkoe, D.J., Hedden, T., Buckner, R.L., Becker, J.A., Johnson, K.A., 2009. Amyloid deposition is associated with impaired default network function in older persons without dementia. Neuron 63(2), 178-188.
Tang, X., Oishi, K., Faria, A.V., Hillis, A.E., Albert, M.S., Mori, S., Miller, M.I., 2013. Bayesian Parameter Estimation and Segmentation in the Multi-Atlas Random Orbit Model. PLoS One 8(6), e65591.

van Bergen, J.M., Hua, J., Unschuld, P.G., Lim, I.A., Jones, C.K., Margolis, R.L., Ross, C.A., van Zijl, P.C., Li, X., 2016a. Quantitative Susceptibility Mapping Suggests Altered Brain Iron in Premanifest Huntington Disease. AJNR Am J Neuroradiol 37(5), 789-796.

van Bergen, J.M., Li, X., Hua, J., Schreiner, S.J., Steininger, S.C., Quevenco, F.C., Wyss, M., Gietl, A.F., Treyer, V., Leh, S.E., Buck, F., Nitsch, R.M., Pruessmann, K.P., van Zijl, P.C., Hock, C., Unschuld, P.G., 2016b. Colocalization of cerebral iron with Amyloid beta in Mild Cognitive Impairment. Sci Rep 6, 35514.

Vandenberghe, R., Van Laere, K., Ivanoiu, A., Salmon, E., Bastin, C., Triau, E., Hasselbalch, S., Law, I., Andersen, A., Korner, A., Minthon, L., Garraux, G., Nelissen, N., Bormans, G., Buckley, C., Owenius, R., Thurfjell, L., Farrar, G., Brooks, D.J., 2010. 18F-flutemetamol amyloid imaging in Alzheimer disease and mild cognitive impairment: a phase 2 trial. Ann Neurol 68(3), 319-329.

Wu, B., Li, W., Avram, A.V., Gho, S.M., Liu, C., 2012a. Fast and tissue-optimized mapping of magnetic susceptibility and T2* with multi-echo and multi-shot spirals. Neuroimage 59(1), 297-305.

Wu, B., Li, W., Guidon, A., Liu, C., 2012b. Whole brain susceptibility mapping using compressed sensing. Magn Reson Med 67(1), 137-147.

Zeineh, M.M., Chen, Y., Kitzler, H.H., Hammond, R., Vogel, H., Rutt, B.K., 2015. Activated iron-containing microglia in the human hippocampus identified by magnetic resonance imaging in Alzheimer disease. Neurobiology of Aging.

	Whole sample	*Younger-old*	*Oldest-old*
A) Demographics			
N (M/F)	80 (54/26)	36 (21/15)	44 (33/11)
Age	79.20 ± 11.80	67.75 ± 7.75	88.57 ± 2.69 **
Education	14.99 ± 2.85	15.92 ± 2.61	14.23 ± 2.84 **
ApoE-e4 carriers (%)	17 (21%)	11 (31%)	6 (14%)
B) Neuropsychology			
MMSE	28.99 ± 1.10	29.44 ± 0.81	28.60 ± 1.17 **
VLMT: delayed recall	7.93 ± 3.99	8.58 ± 3.93	7.43 ± 4.02 **
Boston Naming Test	14.43 ± 0.77	14.73 ± 0.45	14.21 ± 0.89 **
Trail making test B/A	2.61 ± 1.41	2.17 ± 0.70	2.98 ± 1.71 **
CERAD: Word list recall	6.99 ± 1.93	7.79 ± 1.32	6.36 ± 2.12 **
CERAD: Word list recognition	9.77 ± 0.65	9.76 ± 0.61	9.78 ± 0.69
CERAD: Word list learning	8.23 ± 1.39	8.82 ± 0.98	7.76 ± 1.49 **
CERAD: Fluency	21.54 ± 6.91	24.36 ± 5.61	19.37 ± 7.08 **
Stroop Interference: color-word	32.60 ± 11.26	27.91 ± 7.50	36.48 ± 12.40 **

Table 1: *Overview of sample A) demographics and B) neuropsychological test performance measures as mean ± STD. * = significant difference (two-sample T-test) between the oldest-old and younger-old with $p < 0.05$, ** = $p < 0.01$ and *** = $p < 0.001$.*

	Statistics, correlation analysis	
	β-amyloid plaque burden	***Iron-load***
A) Regional volume		
Amygdala	p=0.01 r=0.28 *	p=0.94 r=-0.03
Insula	p=0.99 r=0.00 †	p=0.02 r=0.28 *
Hippocampus	p=0.55 r=-0.08	p=0.74 r=0.06
Entorhinal Cortex	p=0.08 r=0.21 †	p=0.01 r=-0.30 *
Frontal Cortex	p=0.99 r=0.00	p=0.54 r=0.09
Temporal Cortex	p=0.34 r=0.12	p=0.10 r=0.19
Parietal Cortex	p=0.18 r=-0.16	p=0.03 r=0.26 *
Occipital Cortex	p=0.99 r=-0.02	p=0.68 r=0.06
Neocortex	p=0.90 r=-0.04	p=0.11 r=0.19
B) SVCD-burden (WMH-scores)		
Amygdala	p=0.06 r=0.22	p=0.07 r=-0.22
Insula	p=0.07 r=0.22	p=0.42 r=-0.12
Hippocampus	p=0.99 r=0.01	p=0.98 r=0.04
Entorhinal Cortex	p=0.05 r=0.23 *	p=0.05 r=-0.24 *
Frontal Cortex	p=0.05 r=0.23 *	p=0.06 r=-0.23
Temporal Cortex	p=0.17 r=0.17	p=0.03 r=-0.26 *
Parietal Cortex	p=0.23 r=0.16	p=0.01 r=-0.29 *
Occipital Cortex	p=0.48 r=0.11	p=0.12 r=-0.19
Neocortex	p=0.11 r=0.20	p=0.03 r=-0.26 *

Table 2: *Regional correlation analysis for A) volume and B) SVCD with the respective local β-amyloid plaque burden and iron-load. Indicated are values for the entire sample (n=80), * indicates a significant correlation with p-FDR-corrected < 0.05; † = significant differences in regressions slopes between oldest-old and younger-old using Fisher r-to-z transformation, with p < 0.05.*

	Statistics, pathology-measures by group		
	Whole sample	***Younger-old***	***Oldest-old***
A) Volume (ml)			
Amygdala	3.19 ± 0.04	3.24 ± 0.05	3.14 ± 0.05
Insula	11.83 ± 0.12	12.32 ± 0.15	11.44 ± 0.16 ***
Hippocampus	6.61 ± 0.07	6.95 ± 0.08	6.34 ± 0.08 ***
Entorhinal Cortex	1.74 ± 0.02	1.72 ± 0.04	1.76 ± 0.03
Post Cingulate	13.97 ± 0.12	14.18 ± 0.20	13.81 ± 0.15
Thalamus	8.63 ± 0.08	9.04 ± 0.09	8.29 ± 0.10 ***
Caudate	6.70 ± 0.08	6.77 ± 0.13	6.65 ± 0.11
Putamen	6.65 ± 0.07	6.91 ± 0.09	6.44 ± 0.10 **
Globus Pallidus	2.46 ± 0.03	2.56 ± 0.04	2.38 ± 0.03 ***
Frontal Cortex	146.07 ± 0.78	148.31 ± 1.16	144.24 ± 0.97 *
Temporal Cortex	111.56 ± 0.76	114.40 ± 1.02	109.24 ± 0.97 ***
Parietal Cortex	76.37 ± 0.45	77.64 ± 0.51	75.33 ± 0.66 *
B) β-amyloid plaque burden (18F-Flutemetamol SUVR)			
Amygdala	1.37 ± 0.02	1.24 ± 0.02	1.47 ± 0.03 ***
Insula	1.38 ± 0.04	1.21 ± 0.03	1.52 ± 0.07 ***
Hippocampus	1.35 ± 0.02	1.28 ± 0.02	1.40 ± 0.03 **
Entorhinal Cortex	1.18 ± 0.02	1.08 ± 0.02	1.26 ± 0.03 ***
Post Cingulate	1.46 ± 0.05	1.31 ± 0.04	1.59 ± 0.08 **
Thalamus	1.77 ± 0.03	1.63 ± 0.03	1.88 ± 0.05 ***
Caudate	1.21 ± 0.04	1.10 ± 0.04	1.30 ± 0.07 *
Putamen	1.65 ± 0.04	1.47 ± 0.03	1.79 ± 0.06 ***
Globus Pallidus	2.35 ± 0.04	2.20 ± 0.04	2.48 ± 0.05 ***
Frontal Cortex	1.32 ± 0.04	1.17 ± 0.04	1.45 ± 0.07 **
Temporal Cortex	1.29 ± 0.03	1.17 ± 0.02	1.38 ± 0.05 **
Parietal Cortex	1.27 ± 0.04	1.20 ± 0.03	1.33 ± 0.06
Neocortex	1.30 ± 0.03	1.19 ± 0.03	1.39 ± 0.06 **
C) Iron-load (susceptibility, ppm)			
Amygdala	0.022 ± 0.001	0.024 ± 0.002	0.021 ± 0.002
Insula	0.009 ± 0.001	0.013 ± 0.001	0.005 ± 0.001 ***
Hippocampus	0.018 ± 0.001	0.018 ± 0.002	0.018 ± 0.001
Entorhinal Cortex	0.049 ± 0.002	0.050 ± 0.002	0.048 ± 0.003
Post Cingulate	0.021 ± 0.001	0.023 ± 0.001	0.019 ± 0.001 **
Thalamus	0.018 ± 0.001	0.018 ± 0.001	0.018 ± 0.002
Caudate	0.074 ± 0.003	0.076 ± 0.003	0.073 ± 0.005
Putamen	0.088 ± 0.004	0.079 ± 0.002	0.096 ± 0.006 *
Globus Pallidus	0.130 ± 0.004	0.134 ± 0.003	0.128 ± 0.006
Frontal Cortex	0.023 ± 0.001	0.025 ± 0.001	0.022 ± 0.001 *
Temporal Cortex	0.021 ± 0.001	0.023 ± 0.001	0.019 ± 0.001 *
Parietal Cortex	0.026 ± 0.001	0.028 ± 0.001	0.024 ± 0.001 **
D) SVCD-burden (WMH-score)			
Whole brain	4.69 ± 1.80	2.36 ± 0.29	6.59 ± 0.62 **

Supplementary Table 1*: Overview of average structure volume, β-amyloid plaque burden, iron-load and WHM-scores per region and group (mean ± SEM). Group-differences were investigated by independent-sample, two tailed T-test and FDR correction for multiple testing * = p < 0.05, ** = p < 0.01 and *** = p < 0.001.*

	Whole sample	***Younger-old***	***Oldest-old***
A) ***Volume (ml)***			
Amygdala	p=0.09 r=-0.21	p=0.68 r=-0.15	p=0.62 r=-0.14
Insula	p=0.15 r=-0.19	p=0.99 r=0.04	p=0.52 r=-0.16
Hippocampus	p=0.29 r=-0.15	p=0.09 r=-0.21	p=0.94 r=0.09
Entorhinal Cortex	p=0.07 r=-0.21	p=0.55 r=-0.17	p=0.92 r=-0.09
Post Cingulate	p=0.19 r=-0.18	p=0.99 r=0.08	p=0.35 r=-0.19
Thalamus	p=0.33 r=-0.15	p=0.92 r=0.11	p=0.83 r=-0.11
Caudate	p=0.16 r=-0.19	p=0.99 r=0.00	p=0.32 r=-0.20
Putamen	p=0.23 r=-0.17	p=0.66 r=0.15	p=0.55 r=-0.15
Globus Pallidus	p=0.25 r=-0.16	p=0.99 r=-0.07	p=0.99 r=-0.04
Frontal Cortex	p=0.14 r=-0.20	p=0.99 r=0.01	p=0.42 r=-0.18
Temporal Cortex	p=0.15 r=-0.19	p=0.99 r=0.01	p=0.46 r=-0.17
Parietal Cortex	p=0.19 r=-0.18	p=0.99 r=0.02	p=0.28 r=-0.21
Neocortex	p=0.13 r=-0.20	p=0.99 r=-0.02	p=0.40 r=-0.18
B) β-amyloid plaque burden (18F-Flutemetamol SUVR)			
Amygdala	p=0.99 r=0.03	p=0.90 r=-0.11	p=0.99 r=0.04
Insula	p=0.68 r=0.10	p=0.99 r=-0.06	p=0.99 r=-0.03
Hippocampus	p=0.99 r=0.04	p=0.86 r=-0.11	p=0.36 r=-0.19
Entorhinal Cortex	p=0.50 r=0.12	p=0.09 r=0.13	p=0.99 r=0.00
Post Cingulate	p=0.12 r=0.20	p=0.52 r=0.18	p=0.60 r=0.14
Thalamus	p=0.43 r=0.13	p=0.17 r=-0.21	p=0.83 r=0.11
Caudate	p=0.99 r=0.04	p=0.70 r=-0.14	p=0.66 r=0.13
Putamen	p=0.27 r=0.16	p=0.99 r=0.08	p=0.99 r=0.03
Globus Pallidus	p=0.45 r=0.13	p=0.99 r=0.01	p=0.99 r=0.00
Frontal Cortex	p=0.28 r=0.16	p=0.99 r=0.03	p=0.86 r=0.10
Temporal Cortex	p=0.38 r=0.14	p=0.57 r=0.16	p=0.92 r=-0.10
Parietal Cortex	p=0.99 r=0.06	p=0.99 r=0.08	p=0.88 r=-0.10
Neocortex	p=0.17 r=0.19	p=0.59 r=0.16	p=0.74 r=-0.12

Supplementary Table 2: *Regional correlation between years of education and A) structure volume and B) local β-amyloid plaque burden.*

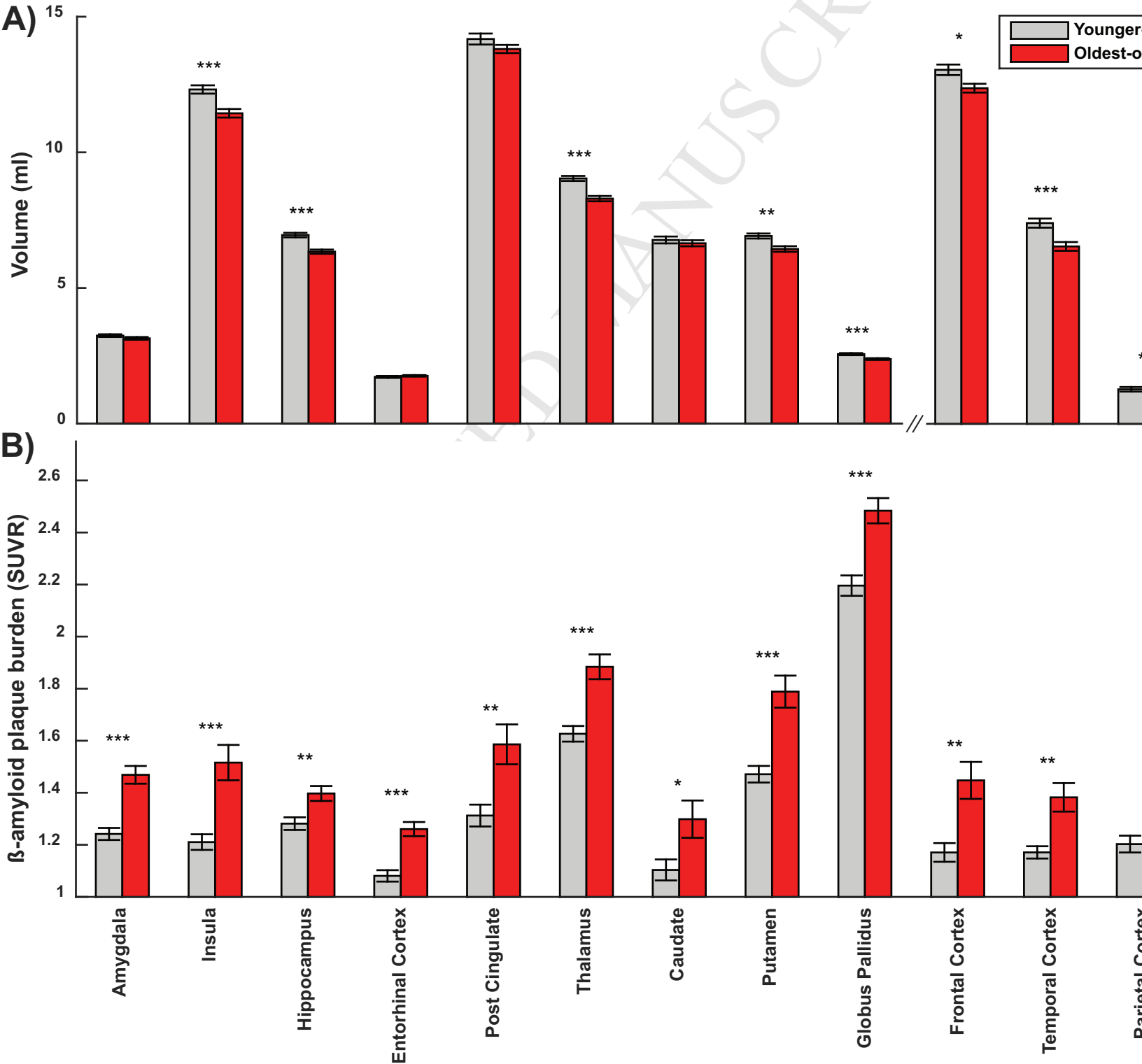

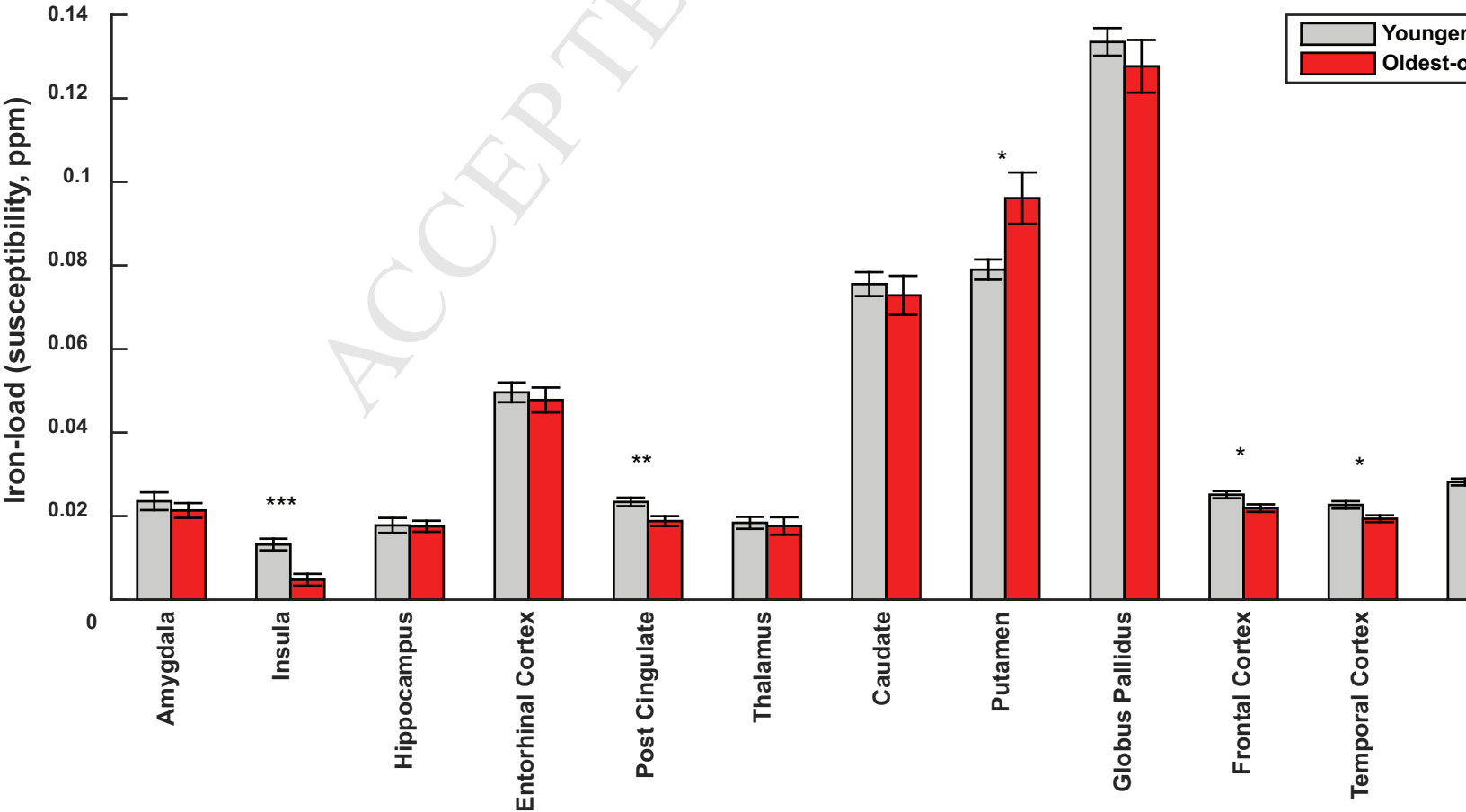

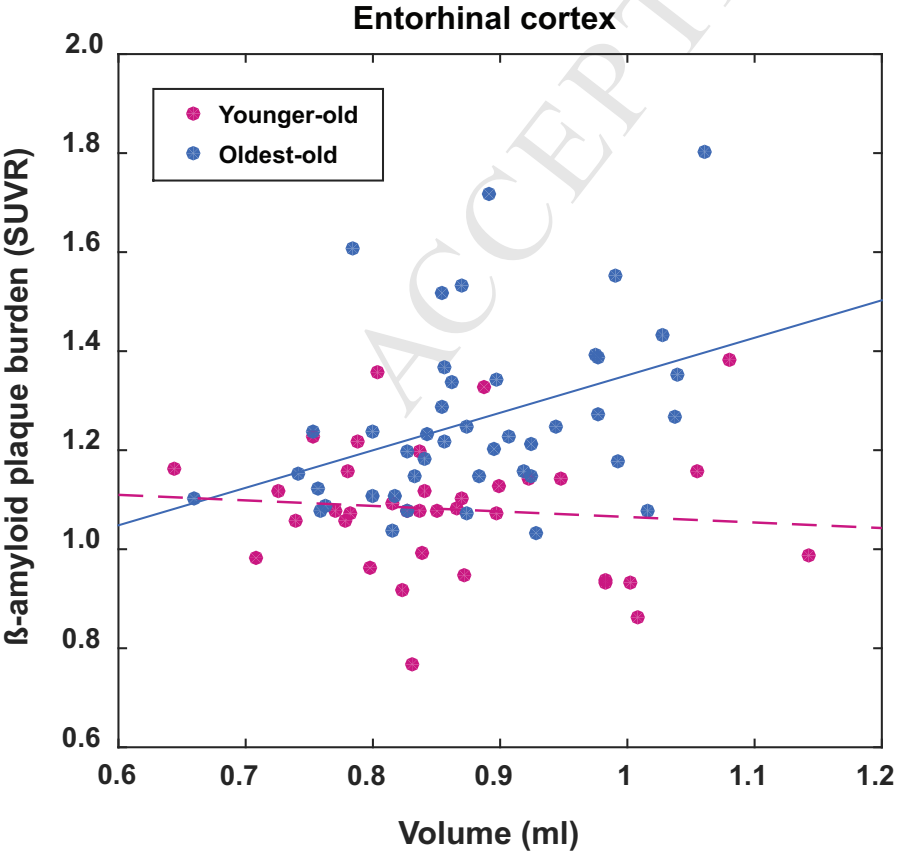

Highlights

- Combined PET-MRI was used to investigate maintained cognition at highest age
- QSM measures of cortical iron load were lower in cognitively unimpaired oldest-old
- Low cortical iron constitutes low vulnerability to aging-associated neuropathologies
- In the oldest-old, high entorhinal cortex volume was associated with high β-Amyloid

All authors contributed to and have approved the final manuscript. All sources of funding and personal relationships relevant to this study are disclosed. None of the authors has published or submitted any related papers from the same study.

Competing Financial Interests statement

Dr. Peter van Zijl is a paid lecturer for Philips Healthcare and is the inventor of technology that is licensed to Philips. This arrangement has been approved by The Johns Hopkins University in accordance with its Conflict of Interest policies. Dr. Paul G. Unschuld is supported by a GE-healthcare grant for investigator initiated research. This funding is in accordance with guidelines issued by the University of Zürich.

Acknowledgments

We thank all subjects for their study participation and Esmeralda Gruber for help with patient recruitment and study administration. This work was funded by the Swiss National Science Foundation (Schweizerischer Nationalfonds, SNF), the Mäxi foundation, the Clinical Research Priority Program (CRPP) of the University of Zürich on Molecular Imaging (MINZ), a grant from the National Institutes of Health (NIBIB) P41 EB015909, investigator initiated research support by GE-healthcare (114-2014-IIR-0075 and 114-2014-IIR-0076), and institutional support from the Institute for Regenerative Medicine (IREM), University of Zürich, Switzerland. This work was supported by the Zürich Impulse Program for the Sustainable Development of Mental Health Services.